RECORD COPY
DO NOT TAKE FROM THIS ROOM

SAND81-0116
UNLIMITED RELEASE
UC-20A

DYNAMICS OF VAPORIZATION AND DISSOCIATION DURING TRANSIENT SURFACE HEATING, WITH APPLICATION TO VACUUM ARCS

DAVID A. BENSON

PRINTED FEBRUARY 1981

Sandia National Laboratories

3-Q(3-80)

Issued by Sandia Laboratories, operated for the United States Department of Energy by Sandia Corporation.

NOTICE

This report was prepared as an account of work sponsored by the United States Government. Neither the United States nor the Department of Energy, nor any of their employees, nor any of their contractors, subcontractors, or their employees, makes any warranty, express or implied, or assumes any legal liability or responsibility for the accuracy, completeness or usefulness of any information, apparatus, product or process disclosed, or represents that its use would not infringe privately owned rights.

Printed in the United States of America

Available from
National Technical Information Service
U. S. Department of Commerce
5285 Port Royal Road
Springfield, VA 22161

Price: Printed Copy $4.50; Microfice $3.00

UC-20A

SAND81-0116
Unlimited Release
Printed February 1981

DYNAMICS OF VAPORIZATION AND DISSOCIATION DURING TRANSIENT SURFACE HEATING, WITH APPLICATION TO VACUUM ARCS

David A. Benson
Thermomechanical and Physical Division 5534
Sandia National Laboratories
Albuquerque, New Mexico 87185

Abstract

This report describes a model of vaporization and dissociation occurring as a result of intense heating over a localized area of a material surface. The balance of heat between the input power and losses due to vaporization, as well as radiation and conduction in the material, are considered. The model includes the effect of binary mass diffusion and changes of surface stoichiometry for multiple component materials. Effects of vapor recondensation are included. The model is then applied to the description of spot heating on a vacuum arc anode through the use of a simple power feedback model. Comparison of surface temperature measurements to model predictions are used to parametrically describe the arc behavior. Finally, extensive parametric analyses showing the effect of material property variations on the arc behavior are described.

TABLE OF CONTENTS

		Page
I.	INTRODUCTION	5
II.	SURFACE HEATING INDUCED VAPORIZATION MODEL	7
	A. A Model for Single Constituent Materials	7
	B. Mass Diffusion Effects in the Surface Material	10
III.	APPLICATION TO VACUUM ARCS	14
	A. Constant Arc Power Calculations	15
	B. Power Variation due to Vapor Flux Feedback	19
IV.	PARAMETRIC STUDIES	27
APPENDIX A.	Listing of the program for surface temperature and vapor flux calculations	45

LIST OF TABLES

		Page
Table I.	Thermal Parameters for assorted metals and hydrides.....	13
Table II.	Input parameters for the arc calculations of Fig. 2.....	17
Table III.	Listing of the time-dependent surface temperatures, heat and vapor fluxes for the calculations of Fig. 2.....	18
Table IV.	Input parameters for the arc calculations of Fig. 3 and listing of the surface temperature, heat and vapor flux results.....	22

LIST OF FIGURES

		Page
Figure 1.	Schematic illustration of the spot heating calculations...	8
Figure 2.	Calculated surface temperature (relative to 300 K) as a function of time for a constant power input over a 6.8 μs duration.....	16
Figure 3.	Calculated surface temperature (relative to 300 K) as a function of time, including the power feedback which constrains the vapor flux values to less than .1 mole/cm^2-s.....	20
Figure 4.	The calculated power into the hydride surface required to maintain the vapor flux below .1 mole/cm-s.....	21
Figure 5.	This comparison illustrates the inconsistency between the observed temperature profiles and the assumption of constant power input to the electrode surface during the pulse, when the effect of hydrogen depletion from the surface material is considered.....	25
Figure 6.	A series of temperature profiles calculated for indicated values of thermal diffusivity.....	28
Figure 7.	Calculated power profiles which limit the vapor flux at the surface to .1 moles/cm^2-s over the arc duration for the indicated values of thermal diffusivity in cm^2/s.....	29
Figure 8.	Calculations showing the effect on the surface temperature as a function of time of different values for initial power input to the arc.....	31
Figure 9.	Four temperature profiles calculated for the indicated values of accommodation coefficient.....	32
Figure 10.	Four calculations showing the effect of mass diffusion on the thermal history of the surface.....	34
Figure 11.	The effect of the limiting flux parameter on the calculated temperature profiles.....	35
Figure 12.	Four calculations showing the effect of concentration variations on the surface temperature profiles for an arc heated surface.....	37
Figure 13.	Examples of vacuum arc discharge heating of anode spots on surfaces composed of different materials.....	39
Figure 14.	Additional examples of heating profiles for anode spots found on the indicated materials.....	40

I. INTRODUCTION

Prediction of thermal behavior in materials undergoing intense surface heating is of interest for applications where materials are exposed to non-penetrating energy sources such as lasers or low-energy electron beam devices. Although applicable to other modes of heating, the calculational techniques described in this report will be used to examine the transient electrical discharge heating which occurs at the electrodes of vacuum arc devices. Particular emphasis will be placed on anode phenomena in this work. These discharge events are used for electrical switching, arc heating and for pulsed ion sources in accelerator technology.

The thermal behavior of an electrode containing a single material species has been discussed in work by Grissom and Newton,[1] by Cobine[2], as well as others. In this report, a model is described which extends the previous work to dissociation and vapor production occurring in binary materials. To do this, the effects of mass diffusion and surface stoichiometry changes must be considered. Addition of these, as well as the effects of vapor recondensation, to the thermal model will be described.

One application in which these features are important is for the pulsed hydrogen ion source where thermal dissociation of a hydride material is used. Examples of thermal transients calculated for hydride materials will be described in Section III. Thermal decomposition of other binary materials, such as lithium in carbon, are potential sources of other ions as well. In these applications, the neutral vapor flux and the related ion production have been found to be directly determined by the electrode surface temperature.[1,2] Thus, a model will be presented in the next section to describe the temperature-time behavior for a variety of different electrode

materials and arc conditions. Emphasis will be on the submillisecond time interval.

The calculations involve the solution of coupled equations for heat transfer, mass loss by dissociation and vaporization, diffusion of mass species within the material and the effect of stoichiometry changes on the vaporization. Because of the heat transfer coupling to the thermochemical and mass diffusion effects in this problem, the use of standard numerical heat transfer computer codes is not possible without extensive rewriting of such codes. Thus, a relatively simple numerical code specialized for the spot surface heating problem has been developed. The thermodynamics of decomposition and diffusion, as well as the source heating terms have been parameterized. The values for these parameters are obtained through comparison to arc experiments rather than by attempting to describe the heating with calculations of arc plasma phenomena. These comparisons to experiments, as well as a study of parametric variations and their effects on the electrode surface temperatures will be described.

The first section describes a thermophysical model of heat transfer and dissociation resulting from spot surface heating. Next, extensions of this model for binary materials will be discussed, followed by application of this model to a vacuum arc. Finally, a series of calculations which show the effect of parametric and material variations will be described to illustrate the thermal arc electrode phenomena.

II. SURFACE HEATING INDUCED VAPORIZATION MODEL

A. A Model for Single Constituent Materials

The model in this section describes the heat transfer within a semi-infinite solid. The material is initially at a temperature, T_o, and subjected to heating over a circular surface area of radius, a. The configuration for these calculations is shown in Figure 1. Power input to the surface is assumed to be uniform over the circular area and may have any specified variation as a function of time. The heat input to the surface in this model is balanced by several dissipation terms. These are, first, the conduction of heat into the bulk of the material below the heated spot. Second, as the surface temperature of the material rises, additional heat losses from dissociation and/or vaporization of the surface material occur. Third, the loss of radiant energy from the surface is calculated, although for most short duration anode heating events considered later this term is small compared to the evaporative and conductive losses.

The heat transfer portion of this problem may be solved analytically using an equation from Carslaw and Jaeger[4]. The surface temperature at the center of the heated area is expressed for an arbitrary time dependent power input to the surface by,

$$T(t) = T_o + A \int_0^t \frac{\dot{q}(t - \tau)}{\sqrt{\tau}} \, d\tau$$

where

$$A = \frac{1}{\rho c \sqrt{\pi D}} \quad [1 - \exp(-a^2/4Dt)]$$

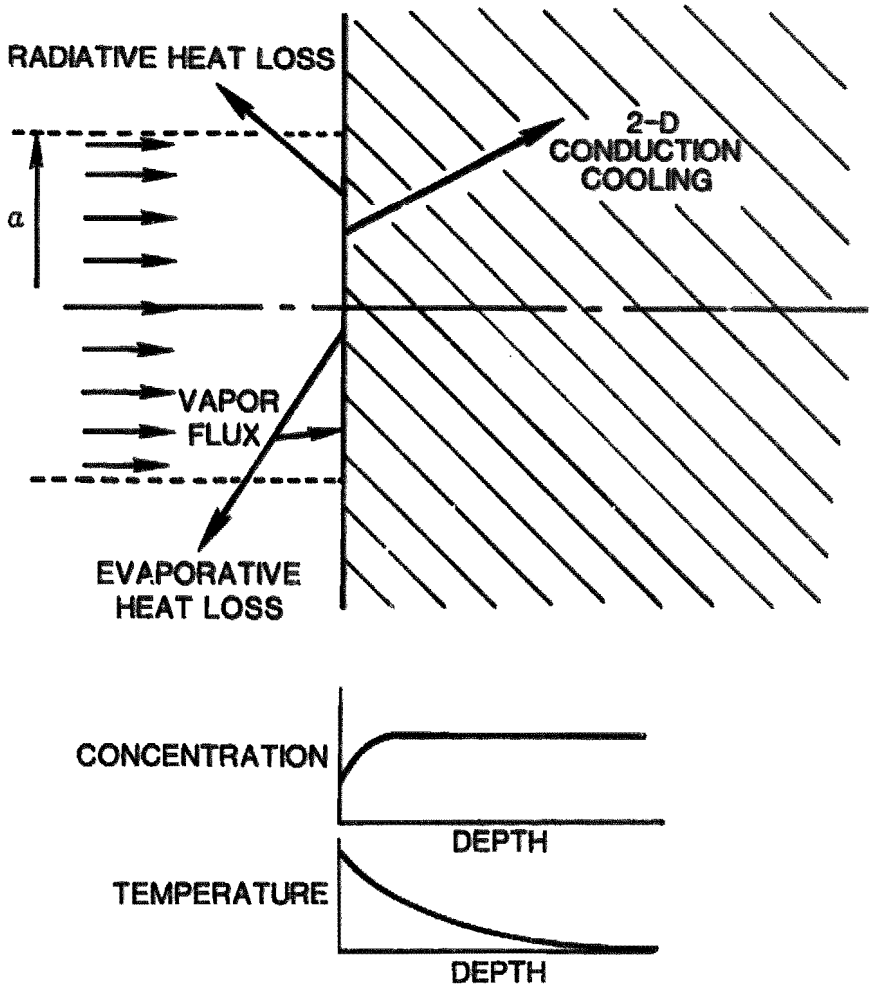

Figure 1. Schematic illustration of the spot heating calculations. Power is input to the surface over an area of radius "a" where the temperature rise of the surface is balanced by heat conduction into the material and by radiative and evaporative heat losses. For binary media, effects due to changes in surface concentration of the evaporating species are also included.

In this equation D is the thermal diffusivity of the material through which heat is being conducted, ρ is it's density, and c is the material heat capacity. The term $\dot{q}(t)$ is the net power input to the surface.

We assume that the power input to the surface to be composed of a source term $\dot{Q}(t)$ and a loss term $\dot{L}(t)$. The source term $\dot{Q}(t)$ is the power input for the problem, for example, the optical input power in a laser heating problem, or the electrical power input to the surface in a vacuum arc calculation.

The loss term for these calculations is the sum of a radiant energy loss term L_1 and a term L_2 describing the loss of energy by evaporation and dissociation at the surface. These are:

$$L_1(t) = \sigma\, T(t)^4 \quad \text{and}$$

$$L_2(t) = \sum_i j_i \left[H_{v_i} + \left(\frac{\partial H_i}{\partial T}\right)_p (T - T_o) \right]$$

where H_{v_i} is the heat of vaporization/dissociation for the i'th species and $\left(\frac{\partial H_i}{\partial T}\right)_P$ is the heat capacity of the i'th component. The vapor flux of the ith component from the surface, j_i, is related to the equilibrium partial pressure P_i by

$$j_i = \alpha_i \frac{P_i}{4} \sqrt{\frac{8}{\pi m_i k T}}$$

where m_i is the molecular mass, and k is Boltzmann's constant. The Langmuir accommodation coefficient, α_i, is surface geometry dependent and expresses the ratio of vapor flux during evaporation from a free surface to the equilibrium Knudsen effusion flux.[6]

The equilibrium partial pressure for the i'th species is related to the temperature-independent heat of vaporization or dissociation, H_v, by

$$\ln P_i = \frac{-H_{v_i}}{RT} + B_i$$

where H_{v_i}/R and B_i are parameters derived from vapor pressure measurements. The temperature used to evaluate the flux and pressure expressions in the spot heating calculations of this report is taken to be the value at the center of the heated spot. While variations of temperature across the heated spot may be important in some cases, the vaporization heat loss in this work acts to attenuate such variations.

The above set of equations form a complete set which may be solved for a given power input. Thus, surface temperatures and vapor flux predictions can be obtained for comparison with experiments.

B. Mass Diffusion Effects in the Surface Material

The surface heating calculations just described are useful for single component materials. In the heating of binary materials, however, they do not account for changes of stoichiometry which may occur at the surface as vaporization preferentially removes the more volatile constituent. This surface depletion must be replenished by mass diffusion from the undepleted subsurface material. In high vapor flux conditions, the bulk mass diffusion rate limits the supply of volatile species to the surface and determines the flux of the volatile component.

To calculate the change in surface composition, the binary diffusion problem is assumed to obey Fick's law. The diffusion of species A in material B is described by

$$\frac{\partial C_A}{\partial t} = D_{AB} \nabla^2 C_A$$

where D_{AB} is the binary diffusion coefficient and C_A is the local concentration of species A. The flux of species A, which is called F_A, may be related to the concentration of C_A by,

$$F_A = D_{AB} \frac{\partial C_A}{\partial x}$$

As an example, the above two equations can be solved to give the surface concentration for the case where a time-independent flux, F, is maintained at the surface for $t > 0$ to give,[5]

$$c(t) = c_o - 2F \sqrt{\frac{t}{\pi D_{AB}}} \quad , \text{ for } c(t) > 0 \quad .$$

This result may be generalized to the case of an arbitrary surface flux f(t) using Duhammel's theorem. Assuming an initial uniform concentration of species A in the material to be C_o, the surface concentration as a function of time becomes

$$c(t) = c_o - \frac{1}{\sqrt{\pi D_{AB}}} \int_o^t f(t - \tau) \frac{d\tau}{\sqrt{\tau}}$$

subject to the constraint that $f(t) = 0$ for $c = 0$.

This expression describes the surface concentration for a given surface vapor flux as a function of time, f(t). In the present work where the depth of the depleted region is very much less than the heated spot diameter, the surface concentration may be evaluated with this one-dimensional expression. Since the flux is described by the equations of the previous section, this

equation allows one to calculate the surface concentration as a function of time.

The relation of equilibrium vapor pressure to the surface stoichiometry is in general complex and must be studied experimentally for the system of interest. The trend of variation, however, may be approximated for many binary media by Sievert's Law as:

$$P(c) = P_o \, (c/c_0)^2$$

where P_o is the equilibrium pressure at concentration c_o. Other functional forms for this concentration dependence will be discussed in Section IV.

When the above expressions for the surface concentration and for the concentration dependence of the equilibrium pressure are combined with the equations of the previous section, they form a complete set of equations to describe the surface temperature as a function time for a given heat input to the surface. The integral equations for temperature and flux must be solved numerically for all but the simplest power input functions. The Fortran program written for this purpose is included in Appendix A.

A number of material parameters must be specified to solve this heat transfer problem. Among these are the vapor pressure equation parameters, the material thermal diffusivity, density and heat capacity. These parameters for several metal and hydride materials are listed in TABLE I. The vapor pressure parameters for the metals were derived from curves published in Ref. 6. The hydride parameters are from Refs. 7 and 8. Heat capacity and thermal diffusivity values have been taken from Ref. 9 and 10.

TABLE I. Thermal parameters for assorted metals and hydrides. The parameters C and D correspond to the expression $\ln P = -(C/T) + D$ where T is in degrees Kelvin and P is in dynes/cm^2. The temperature range listed corresponds to the interval over which these parameters were fit to the tabulation of Ref. 6.

Material	Vapor Pressure Parameters C	D	Range 10^2K	Thermal Diffusivity cm^2/s	Density* g/cm^3	Heat Capacity J/g-^{o}c
Actinium	47276.7	27.3265	11-20	.1*	10.07	.13*
Aluminum	37212.7	27.5937	10-20	.410^H	2.70	.90*
Boron	64.79.3	30.3648	14-30	.017^H	2.34	1.02*
Copper	38.540.5	27.4942	10-21	.806^H	8.96	.386*
Chromium	46506.4	30.4485	10-20	.120^H	7.19	.46*
Erbium	34524.5	26.2578	10-20	.099^H	9.06	.222*
Er Hydride	26931.0	32.2060	4-10	.05*	8.53	.28*
Magnesium	16121.0	25.6193	10-14	.243*	11.4	.13*
Molybdenum	77586.4	30.3586	20-26	.322^H	10.2	.48H
Scandium	39321.2	26.4204	12-16	.093*	3.02	.653
Sc Hydride	24128.0	31.1672	4-10	.04*	2.98	.78*
Silver	32819.0	27.5804	9-18	.628^H	10.5	.235*
Tin	35662.8	26.1146	10-19	.298^H	7.3	.227*
Titanium	54459.2	29.6834	15-20	.0807^H	4.5	.52*
Ti Hydride	19875.0	35.8220	4-10	--	--	--
Tungsten	103635.0	32.1993	25-35	.375*	19.3	.302
Yttrium	48322.4	28.0578	12-17	.162H	4.5	.30*
Zinc	15244.4	27.2537	4-8	.416*	7.14	.39

KEY: $\ln_1[P(\text{dynes/cm}^2)] = -C/T + D$

* - Room Temperature Value
H - Value for 1300K
† - Value for 2000K

III. APPLICATION TO VACUUM ARCS

The surface heating model described up to this point is applicable to any type of surface heating. In this section of the report, the model will be applied specifically to vacuum arc discharges in which intensely heated spots are formed by power incident to the electrode surfaces from the arc. Predicting the surface temperature response to this power input is essential to understanding the performance characteristics of vacuum electrical switching devices and pulsed arc ion sources for use in accelerators.

In such applications, the intense heating of the electrode surfaces results in vapor release from the electrode, some of which is subsequently ionized resulting in a source of charge carriers that affect electrical switch closure or in a source of ions or electrons for use in particle accelerators. The heated spots which form on the cathode surface[11,12] are small rapidly moving areas, typically on the order of one micron diameter where heating occurs, with currents as high as 100 Megamps/cm^2. These high current values produce intense Joule heating of the cathode subsurface in addition to the surface heating from ion bombardment. These highly mobile spots produce sufficient heat and pressure to induce cratering of the cathode surface.[11,12] By contrast, the heating of the anode surface[1,13] occurs over larger spot areas of 50 to 100 microns diameter. The lower power density input to these spots produces a situation in which Joule heating is negligible, so evaporative heat losses and thermal conduction are effective in balancing the thermal input to the surface.[1,13] This allows the anode spots also to remain stationary during a pulsed discharge. Thus, the heat transfer calculations presented in this report are particularly appropriate to the stationary arc anode spot heating problem.

A. Constant Arc Power Calculations

A series of calculations, using the heat transfer equations just discussed, will now be described. The first of these calculations assumes constant power input to the spot during the arc pulse time and no changes in the surface stoichiometry have been included. These assumptions can be tested by comparing the predictions to measurements carried out on an arc heated surface. Input parameters for this calculation are shown in TABLE II. Surface temperatures versus time from the calculation are shown in Fig. 2 and in the tabular listing of TABLE III. The points shown on Fig. 2 are values obtained from infrared radiance measurements on a typical anode spot experiment.[14] To determine these temperatures, an effective emissivity of .35 was assumed for the heated surface material. The pulse duration for the calculation has been selected to match the experiment while the power input to the anode spot was selected in such a way as to match the observed temperature risetime.

Two calculations are shown in Fig. 2. The lower calculation corresponds to a Langmuir accommodation coefficient, α, for the evaporating surface of 0.2 and for the upper curve of 0.3. With this type of calculation, an approximate description of the pulse risetime and peak temperature can be achieved. For both cases, the calculated temperature profiles at the end of the pulse decay much faster than the experimental data from this test. The reason for this is not presently understood. However, the calculations are made for an isolated spot while the experiment actually occurs with mulitple spots in the same region of the anode and may contribute to the slower temperature decay. Possible additional deviations due to a lower substrate thermal diffusivity relative to the surface material in the experiment may contribute as well. Degradation of the thermal contact beneath the heated

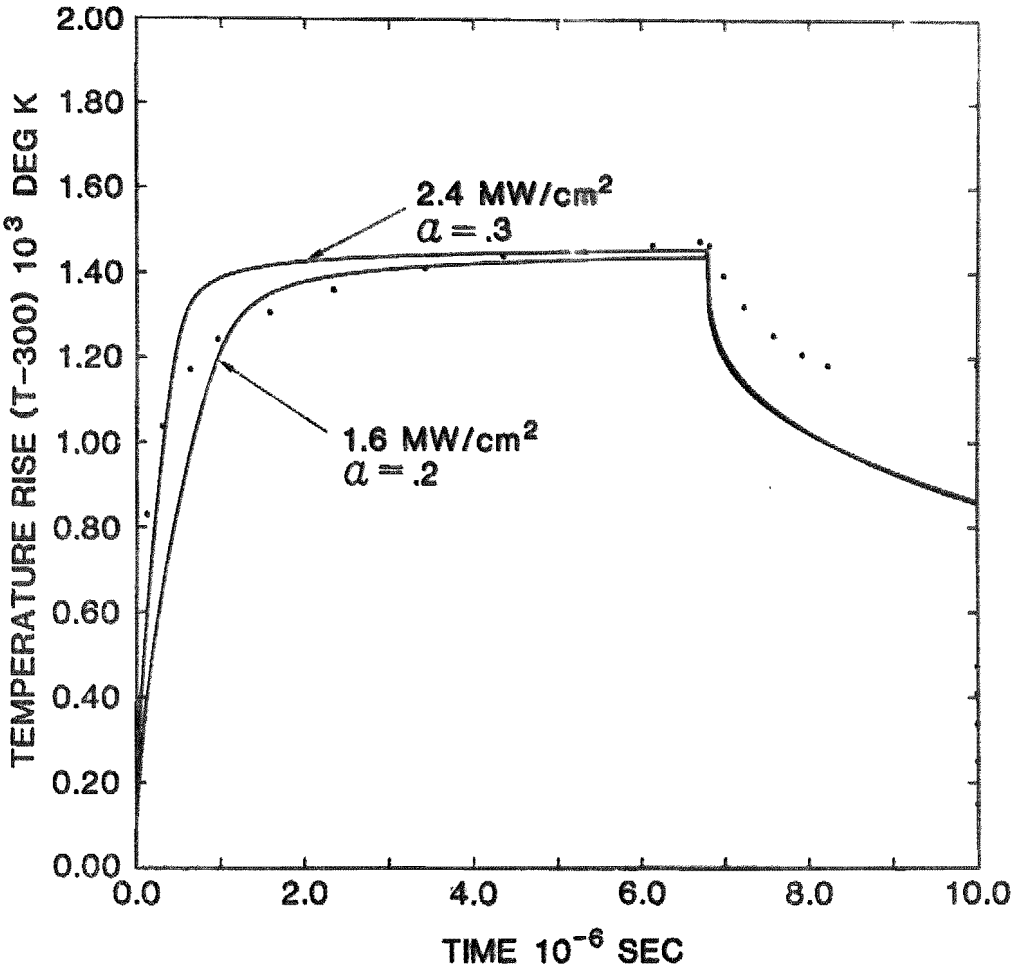

Figure 2. Calculated surface temperature (relative to 300 K) as a function of time for a constant power input over a 6.8 μs duration. The top curve corresponds to an input power of 2.4 MW/cm^2 and an accommodation coefficient of .3 while the lower curve corresponds to 1.6 MW/cm^2 and an accommodation coefficient of .2. These calculations do not account for the depletion of hydrogen from the surface and thus predict abnormally high vapor flux levels. The points on the figure are temperatures derived from the radiance measurements of Robertson.[14]

TABLE II. Input parameters for the arc calculation of Fig. 2.

Thermal Diffusivity = .10 cm^2/s

Specific Heat = 1.36 J/gC

Density = 3.06 g/cm^3

Initial Hydrogenic Concentration = .06 $moles/cm^3$

Pulse Length = 6.8×10^{-6} s

Vapor Pressure Parameters -

Hydrogenic Species	Metal
A = 24100.	A_m = -39321.2
B = 31.261	B_m = 26.4204
M = 2.	M = 45.

TABLE III. Listing of the time-dependent surface temperatures, heat and vapor fluxes for the calculations of Fig. 2. The parameters listed in Table II have been used for these cases. The total output column represents the sum of evaporative and radiative losses.

Surface Temp. C	Time Sec	Energy Flux at Surface: Tot Output W/cm^2	Input W/cm^2	Radiant W/cm^2	Vapor Flux mole/cm^2-s	Hydrogenic Vapor Press dyne/cm^2	Conc moles /cm^3	Metal Vapor Flux mole/cm^2-s
For 1.6 MW/cm^2 power input and α = .2								
97.	.0	.0	$.160\times10^{+7}$	$.001\times10^{+2}$	.0	.0	.060	.0
1216.	$.100\times10^{-5}$	$.147\times10^{+6}$	$.160\times10^{+7}$	$.300\times10^{+2}$	.75	$.05\times10^{8}$	.060	.0
1377.	$.200\times10^{-5}$	$.709\times10^{+6}$	$.160\times10^{+7}$	$.449\times10^{+2}$	3.33	$.22\times10^{8}$	.060	$.62\times10^{-6}$
1407.	$.300\times10^{-5}$	$.909\times10^{+6}$	$.160\times10^{+7}$	$.481\times10^{+2}$	4.42	$.28\times10^{8}$	.060	$.93\times10^{-6}$
1421.	$.400\times10^{-5}$	$.102\times10^{+6}$	$.160\times10^{+7}$	$.497\times10^{+2}$	4.6	$.31\times10^{8}$	.060	$.11\times10^{-5}$
1429.	$.500\times10^{-5}$	$.108\times10^{+6}$	$.160\times10^{+7}$	$.507\times10^{+2}$	4.9	$.33\times10^{8}$	.060	$.12\times10^{-5}$
1435.	$.600\times10^{-5}$	$.113\times10^{+6}$	$.160\times10^{+7}$	$.513\times10^{+2}$	5.2	$.35\times10^{8}$	.060	$.13\times10^{-5}$
1205.	$.700\times10^{-5}$	$.155\times10^{+5}$	.0	$.291\times10^{+2}$	.66	.04	.060	.0
1023.	$.800\times10^{-5}$	$.0174\times10^{+5}$	.0	$.174\times10^{+2}$	.079	.005	.060	.0
926.	$.900\times10a^{5}$	$.004\times10^{+5}$	.0	$.128\times10^{+2}$	.019	.001	.060	.0
For 2.4 MW/cm^2 and α = .3								
146.	.0	.0	$.240\times10^{7}$	$.002\times10^{2}$	.0	.0	.060	.0
1387.	$.100\times10^{-5}$	$.114\times10^{+7}$	$.240\times10^{7}$	$.459\times10^{2}$	$.53\times10^{1}$	$.23\times10^{8}$	.060	$.18\times10^{-5}$
1425.	$.200\times10^{-5}$	$.157\times10^{+7}$	$.240\times10^{7}$	$.502\times10^{2}$	$.72\times10^{1}$	$.32\times10^{8}$	.060	$.18\times10^{-5}$
1438.	$.300\times10^{-5}$	$.174\times10^{+7}$	$.240\times10^{7}$	$.517\times10^{2}$	$.79\times10^{1}$	$.36\times10^{8}$	.060	$.21\times10^{-5}$
1444.	$.400\times10^{-5}$	$.183\times10^{+7}$	$.240\times10^{7}$	$.525\times10^{2}$	$.84\times10^{1}$	$.38\times10^{8}$	.060	$.23\times10^{-5}$
1449.	$.500\times10^{-5}$	$.190\times10^{+7}$	$.240\times10^{7}$	$.530\times10^{2}$	$.86\times10^{1}$	$.39\times10^{8}$	.060	$.24\times10^{-5}$
1452.	$.600\times10^{-5}$	$.194\times10^{+7}$	$.240\times10^{7}$	$.534\times10^{2}$	$.88\times10^{1}$	$.40\times10^{8}$	.060	$.25\times10^{-5}$
1190.	$.700\times10^{-5}$	$.0199\times10^{+7}$	.0	$.279\times10^{2}$	$.86\times10^{1}$	$.041\times10^{8}$	.060	.0
1020.	$.800\times10^{-5}$	$.002\times10^{+7}$	.0	$.172\times10^{2}$	$.001\times10^{1}$	$.005\times10^{8}$	.060	.0
929.	$.900\times10^{-5}$	.0	.0	$.129\times10^{2}$	.0	$.001\times10^{8}$	.060	.0

region is also possible and may account for the lower rate of cooling in the experiments. Systematic study of a collection of such experiments will be needed to clarify this problem.

While the calculation reproduces the major features of the anode surface temperature profile, predictions of the vapor flux evolved from the surface should also be examined. The surface vapor flux required to balance the power input to the anode spot in this example ranges up to 8.8 moles/cm^2-s. This vapor flux when integrated over the pulse is approximately 3×10^{-5} moles/cm^2 of vapor or the equivalent of deuterium loading in a 5 micron layer of hydride material. This is an unreasonably large volume of vapor for this problem since diffusion of vapor from a 5 micron depth in 7 microseconds would require an effective binary diffusion coefficient for hydrogen in the film material of approximately .1 cm^2/s. Both the predictions of single pulse depletion for a 5 micron layer and the requirement for a diffusion coefficient of this magnitude are in gross disagreement with experiments. Multiple pulse tests of layered hydride materials show no such depletion.[15] Also extrapolation of the lower temperature work by Weaver[16] suggests binary diffusion coefficients are 3 to 4 orders of magnitude smaller than the .1 value for temperatures in the range of the arc anode spots.

Therefore, to gain a more realistic description of arc anode performance with a binary material, the effects of arc power variation with time and of mass diffusion within the heated surface material must be included. These additions to the calculations are described in the next section of the report.

B. Power Variation due to Vapor Flux Feedback

In contrast to the previous calculations which assume a constant specific power input to the anode spot during the pulse, this section will

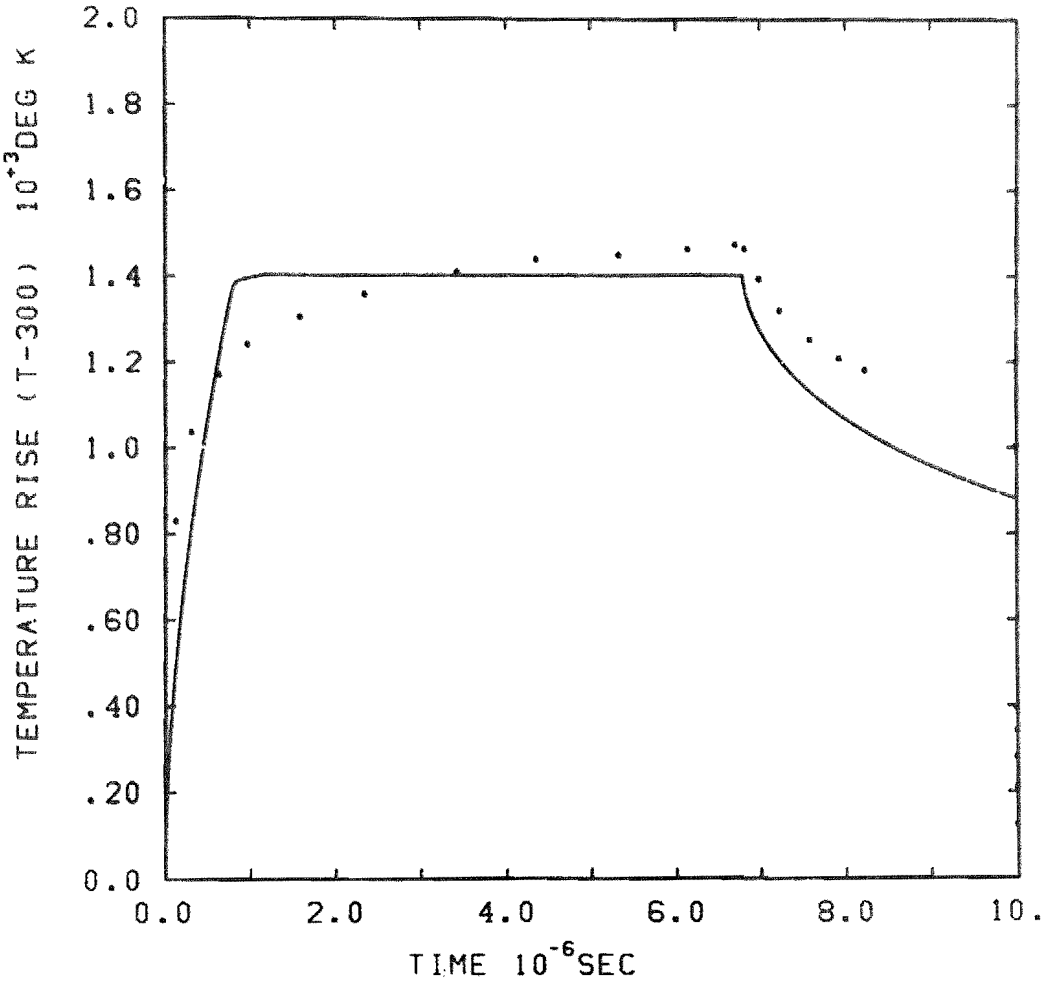

Figure 3. Calculated surface temperature (relative to 300 K) as a function of time including the power feedback which constrains the vapor flux values to less than .1 mole/ cm^2-s. The points are temperature values derived from the radiance measurements of Ref. 14. This calculation also accounts for surface concentration changes.

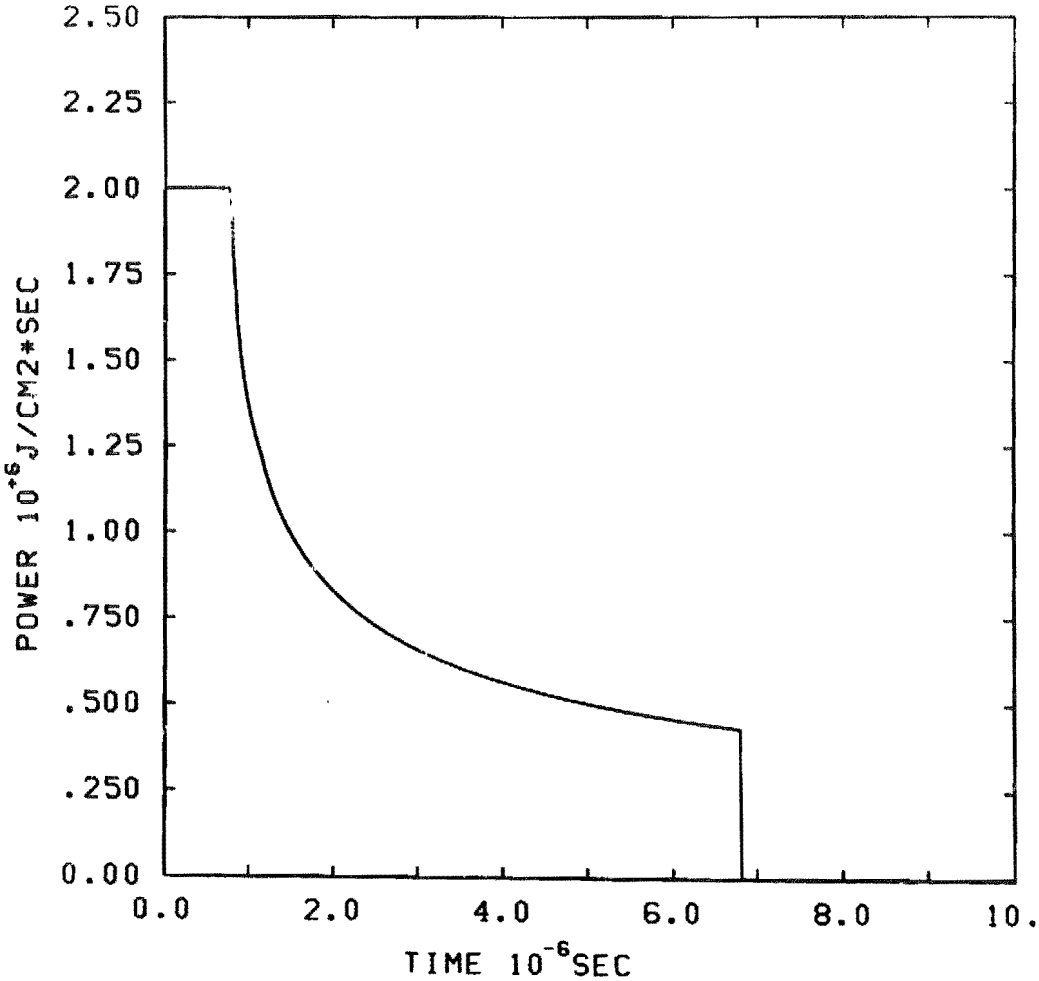

Figure 4. The calculated power into the hydride surface required to maintain the vapor flux below .1 mole/cm-s.

Table IV. Input Parameters for the arc calculations of Fig. 3 and listings of the surface temperature, heat and vapor flux results. The vapor pressure parameters listed in Table II have been used as before. The total output column represents the sum of evaporative and radiative losses.

Thermal Diffusivity = .10 cm^2/s	Initial Hydrogenic Concentration = 0.06 $moles/cm^3$
Specific Heat = 1.36 J/g°C	Mass Diff Coefficient = 1×10^{-4} cm^2/s
Density = 3.06 g/cm^3	Pulse Length = 6.8×10^{-6} s
Initial Power Input = 2×10^6 W/cm^2	Limiting Flux = .1 $moles/cm^2$-s
Accommodation Coef. = .005	

Surface Temp C	Time Sec	Tot Output W/cm^2	Input W/cm^2	Radiant W/cm^2	Vapor Flux $mole/cm^2$-s	Vapor Press $dyne/cm^2$	Conc moles $/cm^3$
121.	.0	.0	2.00×10^6	$.00179 \times 10^2$	.0	.0	.060
1397.	$.100 \times 10^{-5}$	$.221 \times 10^{+5}$	1.36×10^6	$.470 \times 10^2$	.10	$.27 \times 10^8$	.055
1403.	$.200 \times 10^{-5}$	$.220 \times 10^{+5}$	$.827 \times 10^6$	$.476 \times 10^2$	.10	$.27 \times 10^8$	.048
1402.	$.300 \times 10^{-5}$	$.220 \times 10^{+5}$	$.657 \times 10^6$	$.476 \times 10^2$	.10	$.27 \times 10^8$	.044
1402.	$.400 \times 10^{-5}$	$.220 \times 10^{+5}$	$.564 \times 10^6$	$.476 \times 10^2$	.10	$.27 \times 10^8$	.041
1402.	$.500 \times 10^{-5}$	$.220 \times 10^{+5}$	$.502 \times 10^6$	$.476 \times 10^2$	.10	$.27 \times 10^8$	.038
1402.	$.600 \times 10^{-5}$	$.220 \times 10^{+5}$	$.458 \times 10^6$	$.476 \times 10^2$	.10	$.27 \times 10^8$	.035
1268.	$.700 \times 10^{-5}$	$0.760 \times 10^{+5}$	.0	$.343 \times 10^2$	$.31 \times 10^{-1}$	$.080 \times 10^8$	.035
1066.	$.800 \times 10^{-5}$	.0	.0	$.197 \times 10^2$	$.34 \times 10^{-4}$	$.008 \times 10^8$	.040
958.	$.900 \times 10^{-5}$	.0	.0	$.142 \times 10^2$	$.78 \times 10^{-3}$	$.002 \times 10^8$	.043

describe a simple power dependent model. The power variation to be described is based on the effect of increased ion density over the anode surface which produces a feedback to the arc discharge, thereby reducing the power input to the spot surface. While the detailed plasma processes within the electrode gap which lead to this regulation may be difficult to describe, their presence is evident in measurements of vapor flux and arc voltage. The assumption to be made here is that the regulation process occurs to reduce the power input to the surface in such a way that the vapor flux cannot exceed a limiting value, F_o. Actually, the limiting factor is probably the ion density near the spot surface, but for the present, the ionization fraction, is assumed to be sufficiently constant over the length of the pulse that the limit may be expressed by the total vapor flux.

Thus, in further calculations, the assumption of a peak flux value, F_o, will replace the constant power assumption over the pulse duration. For the hydride arc problem, the value, F_o, was selected to be .1 mole/cm^2-s which compares well to the integrated vapor release measured in arc experiments.[15] A constant input power will be assumed for the initial part of the pulse until the limiting flux is achieved. Then the arc power will be assumed to vary in such a way as to never exceed F_o.

Surface temperature predictions from these calculations are shown in Fig. 3. The corresponding variation of power required to avoid exceeding the F_o flux level is shown in Fig. 4 and in Table IV. Again, the initial specific power input to the heated spot was selected to match the pulse risetime as shown by the experimental points in Fig. 2. The peak temperature point is matched by adjusting the accommodation coefficient. This calculation is consistent with measured vapor flux levels and asumes a realistic value for the hydrogen binary diffusion coefficient. In addition,

the main features of the anode spot temperature profile are described. A number of arc events show flat topped pulses similar to this calculation.[15] The temperature ramp of the experimental points in Fig. 3 may be an indication of the reduction in surface stoichiometry occuring during the pulse. To model such behavior requires the variation of hydrogen partial pressure with the material surface stoichiometry to be known. This has been approximated for these calculations with the equilibrium data published for scandium hydride.[7] For these calculations the hydrogen partial pressure was assumed to be independent of concentration for ScH_x with $.6 < x < 1.6$. Outside of this range a variation as the square of the concentration has been assumed. The effect of varying these parameters separately in calculations will be shown in the next section of the report.

The importance of the arc spot power variation during the arc discharge is illustrated in Fig. 5 where a comparison of the constant power and the limiting flux calculations are shown. In these constant power calculations, the hydrogen diffusion and surface concentration variation are included. These necessary features were not included in the previous calculations of Fig. 2. For a constant power input of .7 MW/cm^2 the surface temperature rises to the peak value observed in experiments only at the end of the pulse time. However, as one continues to increase the power to the spot surface, surface depletion and a runaway surface temperature increase occurs as the cooling by hydrogen vaporization is lost. This depletion may be seen in the .8 mW/cm^2 calculation by the steeper slope late in time as depletion is approached. Thus, when realistic hydrogen diffusion is included in the calculation it is not possible to simultaneously match the temperature risetime and peak temperatures with the constant power model.

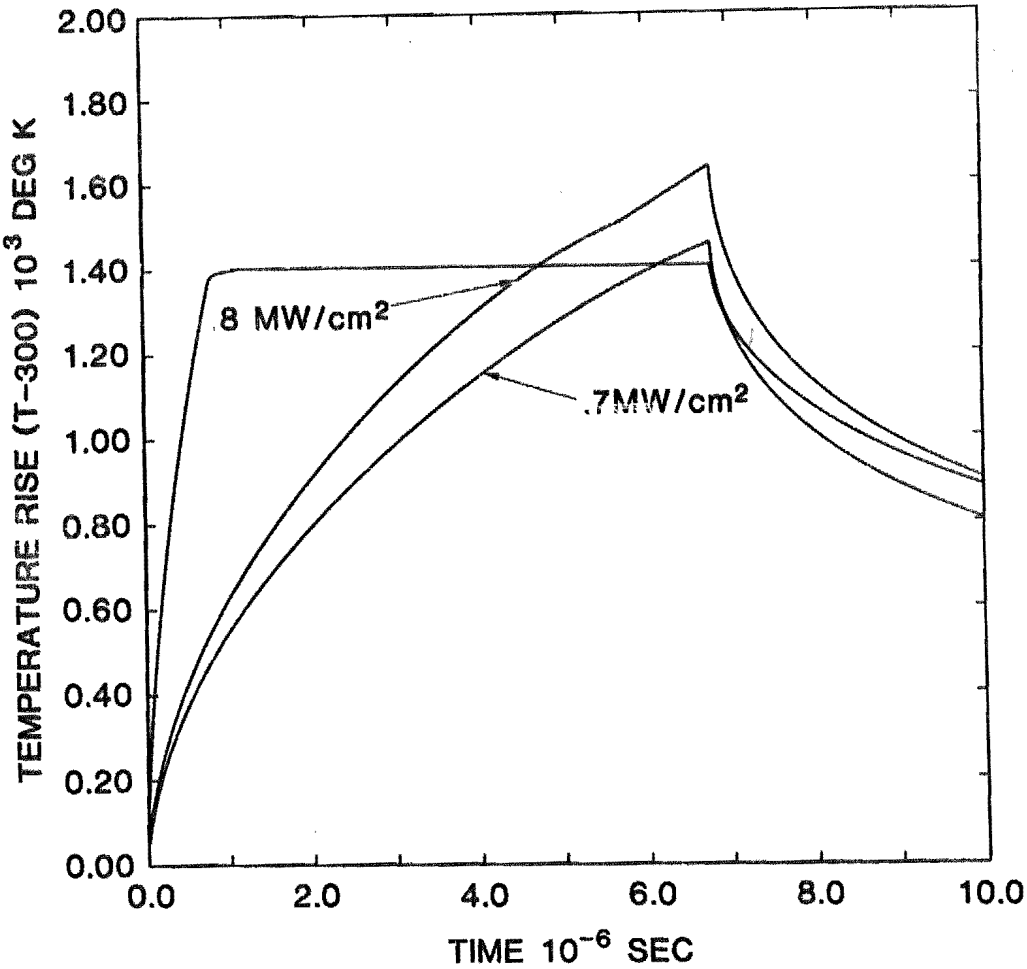

Figure 5. This comparison illustrates the inconsistency between the observed temperature profiles and the assumption of constant power input to the electrode surface during the pulse, when the effect of hydrogen depletion from the surface material is considered. The fast rising temperature profile is the same as the one of Fig. 3 with power feedback. The two slower rising calculations correspond to .7 and .8 MW/cm^2-s power input to the heated spot. The slight upturn in the .8 MW/cm^2-s temperature profile near the end of the pulse is due to the onset of surface depletion and a reduction of the vaporization rate. Any further increase of power in an attempt to match the pulse risetime results in a runaway thermal condition.

To further illustrate phenomena occurring in an arc which may be induced by thermal characteristic of the anode surface, the next section will describe parametric variations of the arc mode calculation to examine each parameter's effect on the anode behavior.

IV. PARAMETRIC STUDIES

The arc model just discussed consistently describes the integrated vapor flux from the anode spot surface, the spot temperature risetime and the peak spot temperatures during the arc event. Although it is a parametric model, it may be used to predict the effect on the arc discharge due to variations in anode characteristics. Summarized in this section is a series of studies in which individual parameters are varied to show their effects on the anode spot temperatures. The parameters and model used to give the result in Fig. 3 have been chosen for the base case in these studies.

The first example shows the effect of the anode material thermal diffusivity on the temperature profiles. For simplicity, a temperature independent value of the thermal diffusivity has been used in each case. The temperature profiles of Fig. 6 show a linear variation of the temperature risetime with thermal diffusivity. This is due to the larger mass of material which must be heated as the diffusivity is increased. The fact that the surface temperature decay at the end of the pulse is nearly independent of diffusivity is a consequence of the deeper penetration of the thermal front, and correspondingly smaller temperature gradients, as the diffusivity is increased. This offsets the higher material thermal diffusivity.

Figure 7 shows the required histories of arc power to the anode surface power input to the surface which are taken from the series of thermal diffusivity calculations. These power histories produce the limiting flux level of .1 moles/cm^2-s over the anode spot for various thermal diffusivities. This rapidly decreasing anode power during the pulse is in qualitative agreement with the observed total power input to the vacuum arc measured

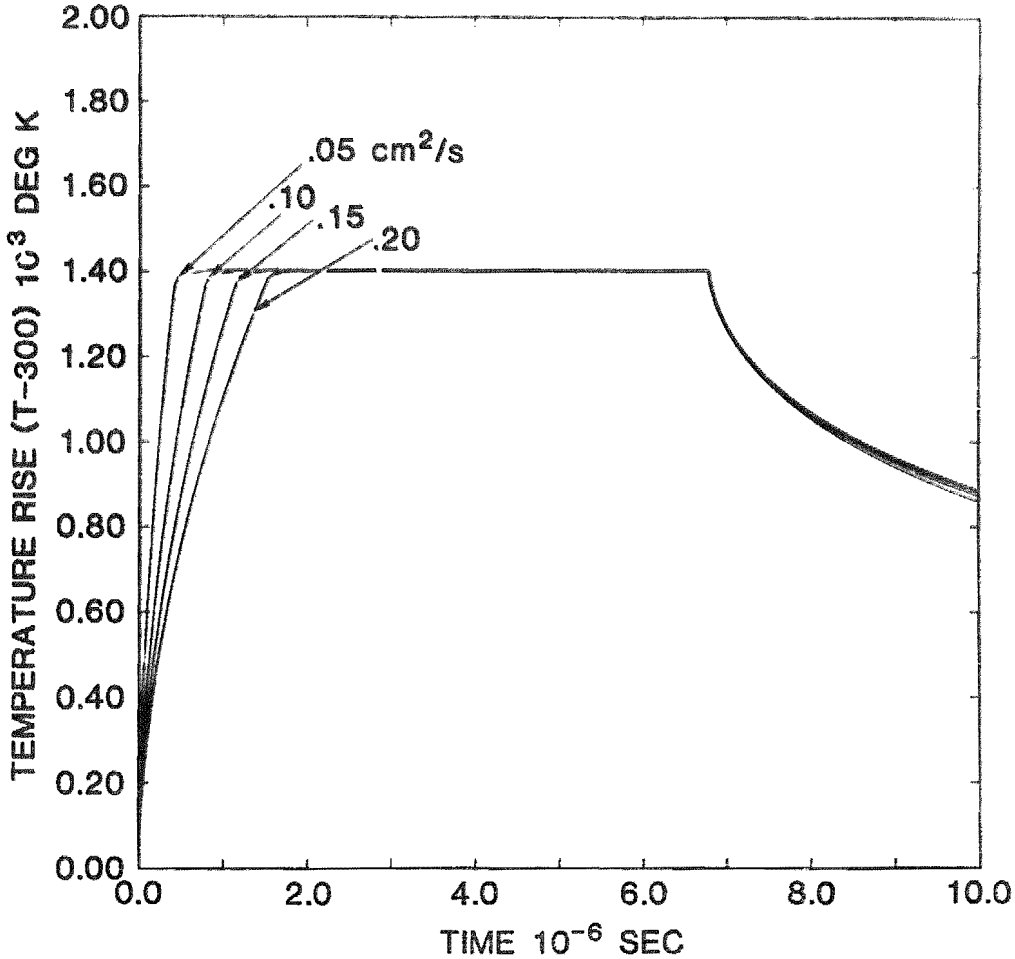

Figure 6. A series of temperature profiles calculated for indicated values of thermal diffusivity.

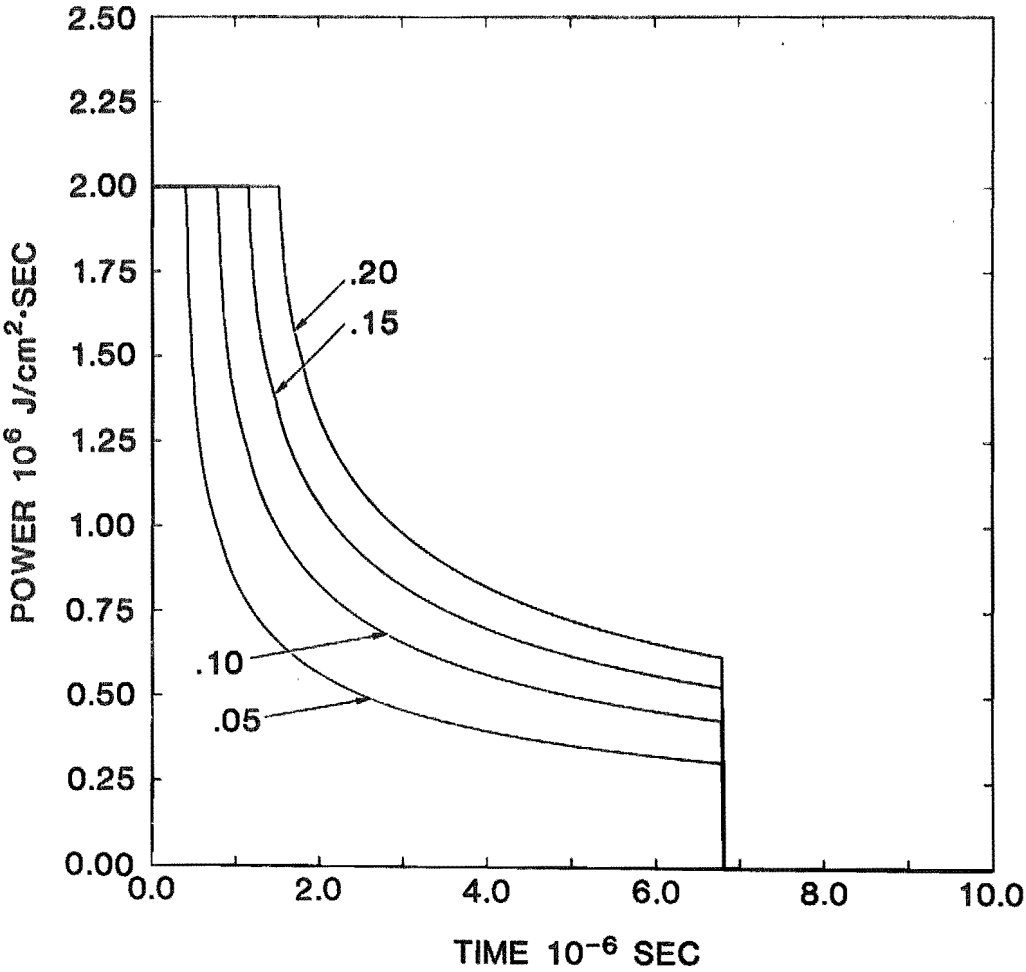

Figure 7. Calculated power profiles which limit the vapor flux at the surface to .1 moles/cm^2-s over the arc duration for the indicated values of thermal diffusivity in cm^2/s.

during an arc discharge[14,15] in which a few stable anode spots account for a major fraction of the arc power.

The results in figure 8 summarize the effect of varying the initial power level to the anode spot. These calculations show that an initial power density of $.5 \times 10^6$ W/cm^2 is inadequate during a short duration discharge to reach the temperature at which the power input becomes controlled by the vapor flux. An initial power input of 2×10^6 W/cm^2 however reproduces the observed risetime in short arc events.[14]

Figure 9 illustrates the effect of the accommodation coefficient on the thermal profiles. The evaporation of material, or in this case dissociation and release of hydrogen, is accompanied by substantial recondensation of material from the vapor phase. The ratio of unrecondensed atoms to the number released is the so called Langmuir accommodation coefficient. For vaporization of common materials,[17] this coefficient has been observed to have values ranging to less than .01 . The value selected for this coefficient has a strong effect on the peak temperature during an arc pulse for a given vapor flux. Thus, the flux necessary to limit the arc input power is coupled to the surface temperature by this coefficient. The accommodation coefficient value of .005 is needed to produce agreement with the experiment shown in Fig. 3. This may be compared, for example, with the sticking probability of .001 to .005 observed by Malinowski in deuterium hydriding studies. That value, although consistent with thermal vaporization from a free surface, may also be influenced, in the vacuum arc case, by the plasma space charge which tends to confine the ions to a region near the anode spot surface. These plasma processes could result in sufficient back pressure to cause recondensation and thereby limit the release of vapor from the surface.

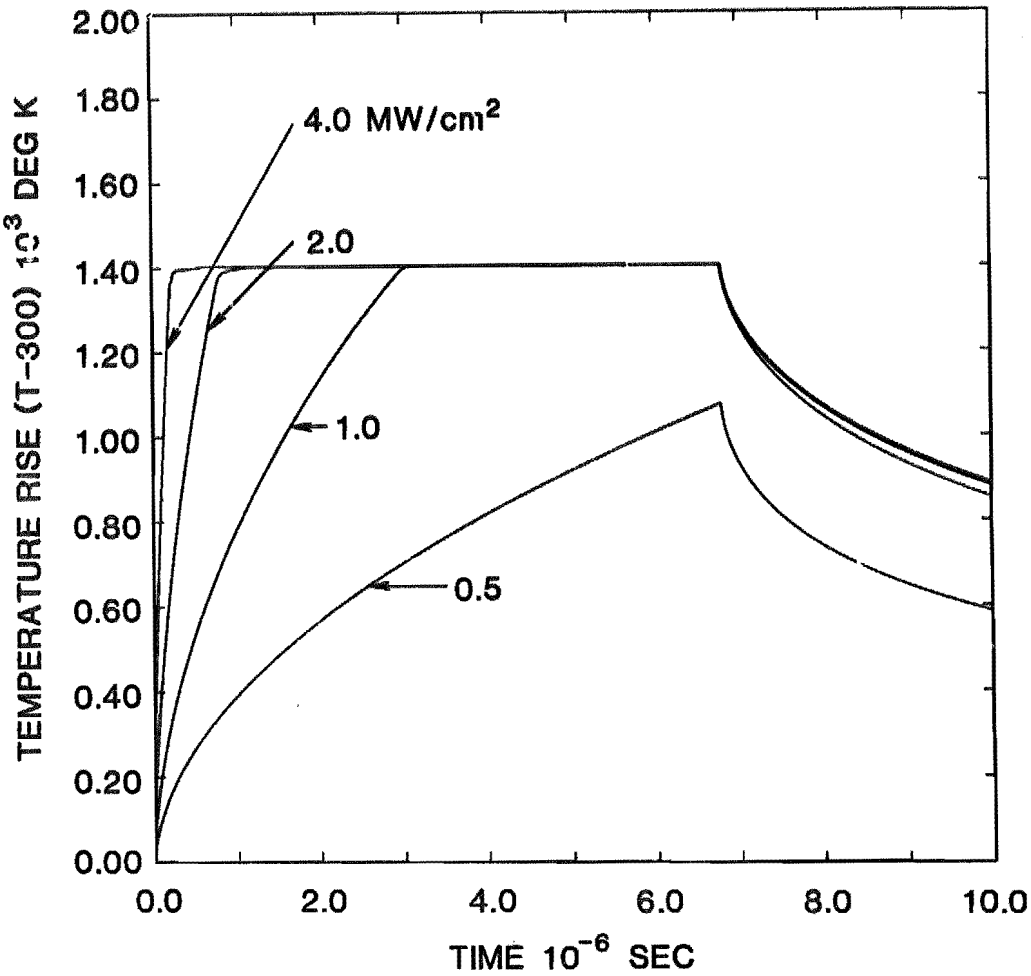

Figure 8. Calculations showing the effect of different values for initial power input to the arc, on the surface temperature as a function of time. Its strong effect on the pulse risetime is evident.

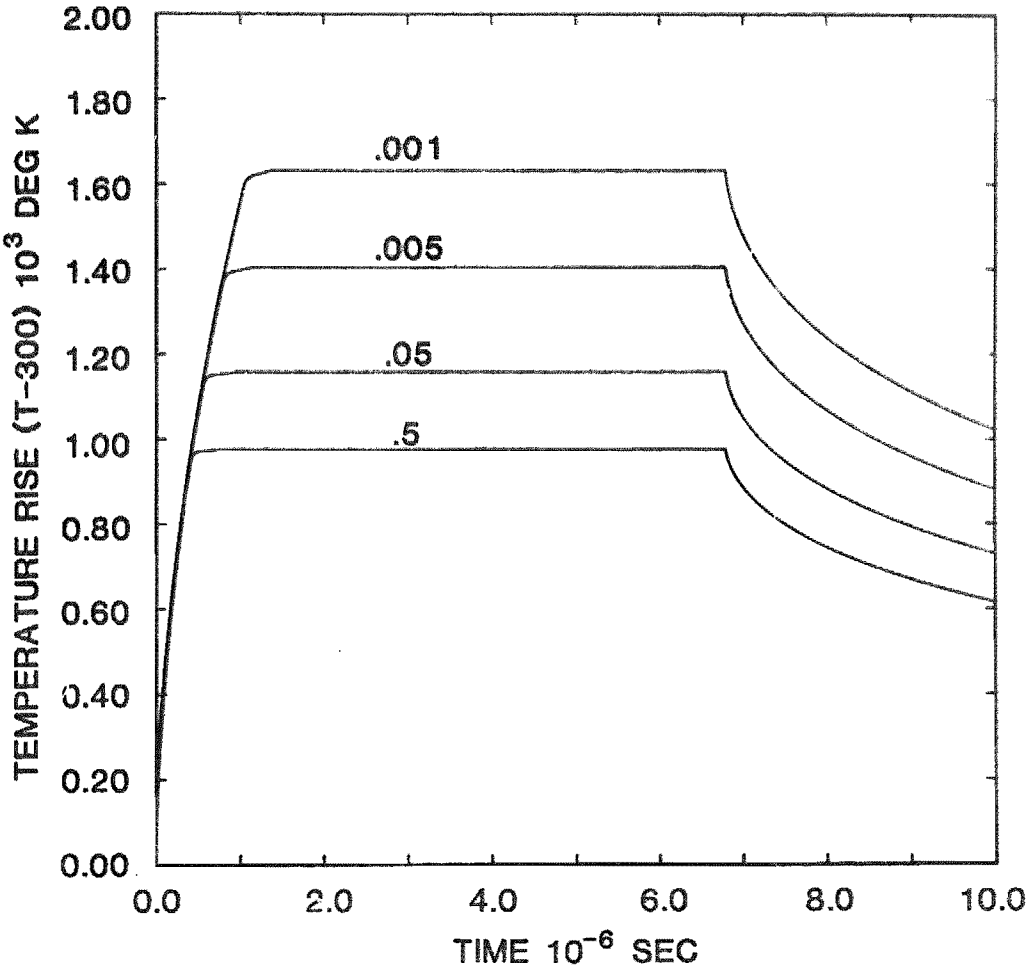

Figure 9. Four temperature profiles calculated for the indicated values of accommdation coefficient. This parameter directly affects the peak surface temperature during the pulse.

As hydrogen is removed from the surface material during the discharge, it must be replenished by diffusion from the volume of undepleted material below the surface. This binary diffusion is parameterized in the present calculations with a temperature and concentration independent diffusion coefficient. Figure 10 shows a sequence of four calculations in which the diffusion coefficient is varied from 1×10^{-3} to 2×10^{-5} cm^2/s. For the lowest value of 2×10^{-5}, the surface material is depleted of hydrogen in half of the power input pulse time. Upon depletion, the cooling by way of hydrogen vaporization is no longer effective and a runaway thermal condition results. This is evidenced by the rapid increase of surface temperature. For binary diffusion coefficients greater than 5×10^{-5} cm^2/s the depletion does not occur and the power regulation process continues throughout the 6.8 microsecond power input pulse. The vapor flux level at which this regulation occurs is constrained to be .1 mole/cm^2-s in each case.

A similar depletion effect can be observed as the limiting flux parameter is changed. This parameter corresponds to the flux value at which power feedback to the arc discharge occurs to stabilize the surface temperature. As the limiting flux parameter is increased for a given diffusion coefficient, the surface material can reach the depleted condition under which thermal runaway occurs. This is shown by the sequence of four calculations in Fig. 11 where the limiting flux is varied from .05 to .22 moles/cm^2-s. The limiting flux value of .1 moles/cm^2-s, selected as the base case value for the calculations in this study, is consistent with measurements of the total vapor flux released in similar arc operations.

As the surface hydride stoichiometry varies, the partial pressure of hydrogenic species over the surface will in general vary for a given temperature. If the variation of vapor pressure with hydrogen concentration

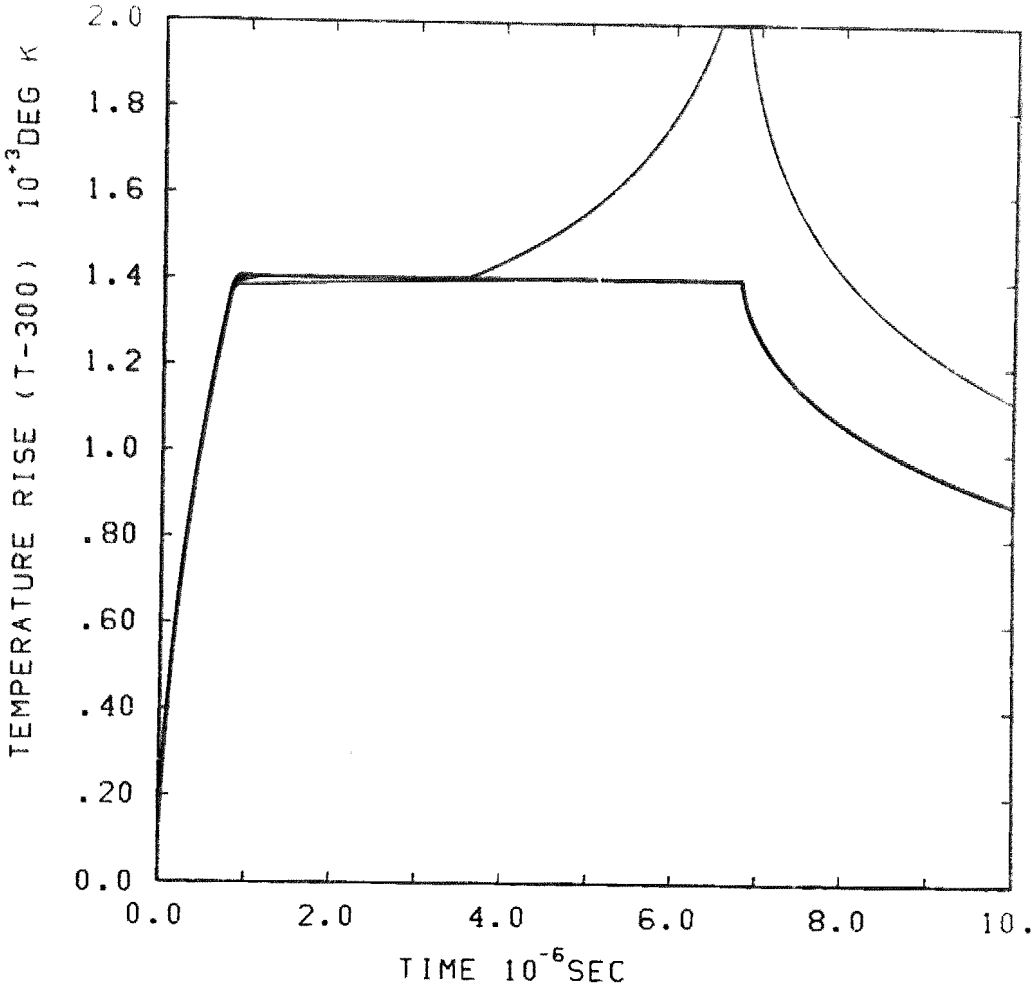

Figure 10. Four calculations showing the effect of mass diffusion on the thermal history of the surface. Three calculations for values of 1×10^{-3}, 1×10^{-4} and 5×10^{-5} cm^2/s give essentially identical profiles. For a value of 2×10^{-5} however, surface depletion occurs resulting in a thermal runaway condition for the surface.

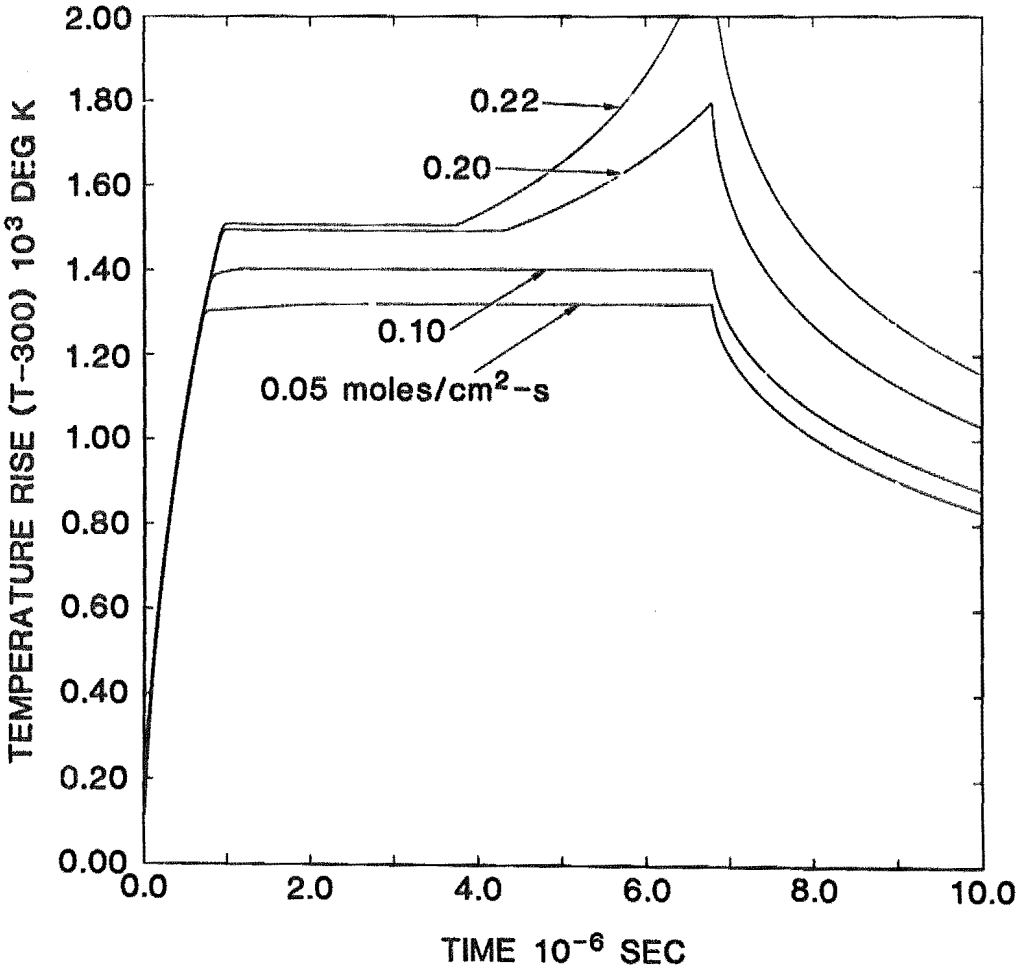

Figure 11. The effect of the limiting flux parameter on the calculated temperature profiles. This parameter affects the peak surface temperature during the arc. More importantly, values of .2 moles/cm^2-s or greater result in a thermal runaway condition caused by the depletion of hydrogenic species in the surface material.

is known, this can be included in the surface heating calculations. In many cases, however, this feature of the hydride properties is not well known. Moreover, evaporation at a surface may be affected by subtle features of the surface material such as contamination by another species.

Figure 12 shows several results from calculations based upon different assumptions for the concentration dependence of the hydrogen partial pressure. Parameters for the baseline calculations of this report used the published results of Lieberman and Wahlbeck[7] for the isothermal relation of the hydrogen partial pressure to the surface stoichiometry. For measurements in the 600°C to 1000°C range, they observed a two phase behavior in ScH_x which gives a concentration independent equilibrium pressure over the range of x values between .6 and 1.6. This concentration behavior has been included in all calculations up to this point. Also, the pressure-temperature behavior of the ScH_x material reported in Ref. 7 has been assumed. Outside of the concentration range just mentioned, the equilibrium pressure P(x) is assumed to vary according to Seivert's Law using $P(x) = P_o(x/x_o)^2$ where P_o is the two-phase equilibrium pressure, where x_o is the phase boundary concentration value.

Calculation 1 of Fig. 12 uses the concentration dependence just described for a problem in which the deuterium concentration of the surface material, C_o, is .067 moles/cm^3 (or x = 1.0). For comparison, calculation 2 assumes C_o to be .04 moles/cm^3. These two calculations show constant temperature segments initially, while the second shows some increase of the anode spot temperature with time that occurs as the surface material falls below the .6 atomic ratio at which the hydrogen partial pressure drops with concentration.

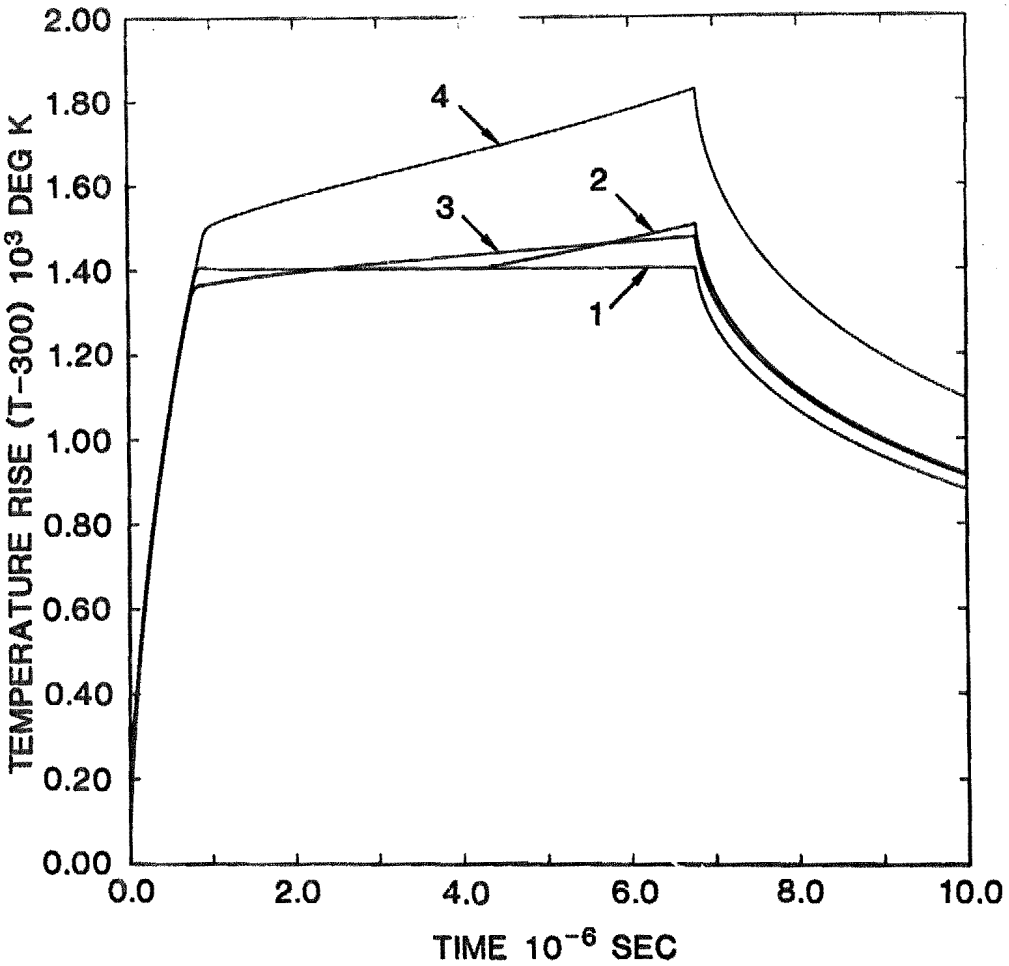

Figure 12. Four calculations showing the effect of concentration variations on the surface temperature profiles for an arc heated surface. Calculations 1 and 2 assume a two-phase region to exist for Sc D_x for x values between .6 and 1.6. Outside this concentration range, a quadratic dependence of vapor pressure on the surface concentration is assumed. The constant temperature segments of each calculation corrsponds to the two-phase region. Curve one is for an initial deuterium concentration, C_o, of .067 moles/cm^3 (or x = 1) while calculation 2 assumes C_o = .04 moles/cm^3. In contrast, curves 3 and 4 assume the quadratic Sieverts law to apply over the entire range of concentrations. For curve 3, C_o = .067 moles/cm^3 and for curve 4, C_o = .04 moles/cm^3. The ramp associated with curve 3 closely resembles the temperature data of Fig. 3 indicating a possible concentration variation during that pulse.

The concentration measurements of Ref. 7, showing the two phase region, were made in the temperature range from 600°C to 1000°C. On the other hand, the anode spot temperatures of interest in these calculations are in the 1400°C range. The higher temperature and pressure of these calculations may lay outside of the two phase boundary seen in the lower temperature work. Some evidence of this can be seen in the narrowing of the 2 phase region with increasing temperature which can be seen in the Ref. 7. data.

Thus additional calculations have been made for comparison purposes which assume no two phase region to exist at the higher temperatures. Instead, a variation of pressure with concentration of $P = P_o(C/C_1)^2$ where $C_1 = .0536$ moles/cm^3 is assumed for the entire concentration range. Calculation 3 has been made using an initial deuterium concentration for the anode material of .067 moles/cm^3 and calculation 4 a value of .04 moles/cm^3. In each case the arc temperature rises during the pulse as the surface hydrogenic concentration is reduced. The ramp of calculation 3 closely matches that of the experimental points in Fig. 3. It is likely that the reduction of anode surface concentration in that experiment accounts for this feature of the thermal pulse.

Effect of Anode Surface Materials

Previous sections of this report have described vacuum arc calculations using hydride materials to simulate experiments of Robertson[14] and Newton[15]. However, the model can be used to illustrate the fast pulse behavior for vacuum arc phenomena in a variety of anode materials. To illustrate the thermal states which can be achieved, a series of calculations will now be described in which the properties of the anode material are varied to represent a collection of different materials in arc applications. To emphasize the effect of thermal properties in the heating profile, these calculations are

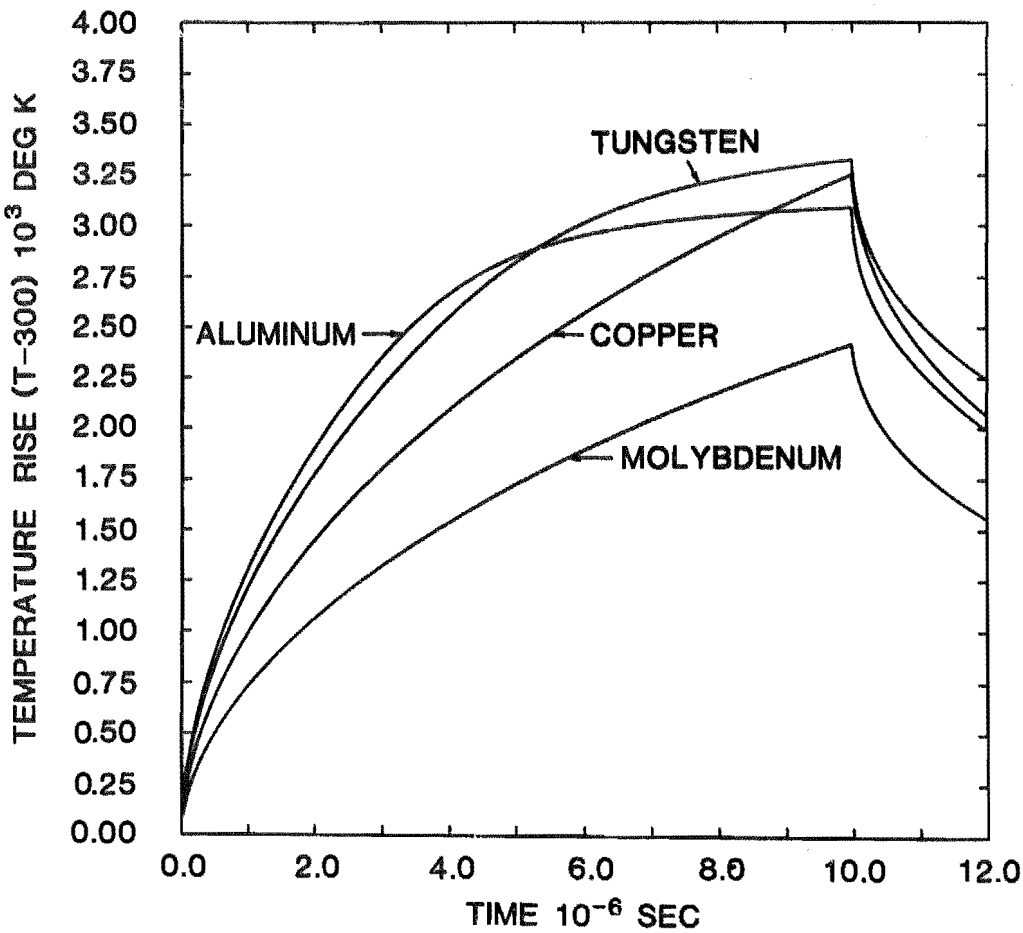

Figure 13. Examples of vacuum arc discharges heating of anode spots on surfaces composed of different materials. In each case, the risetime of the thermal pulse is associated with the heat capacity and thermal diffusivity of the surface, while the limiting of the temperature is reached where vaporization contributes to the surface cooling.

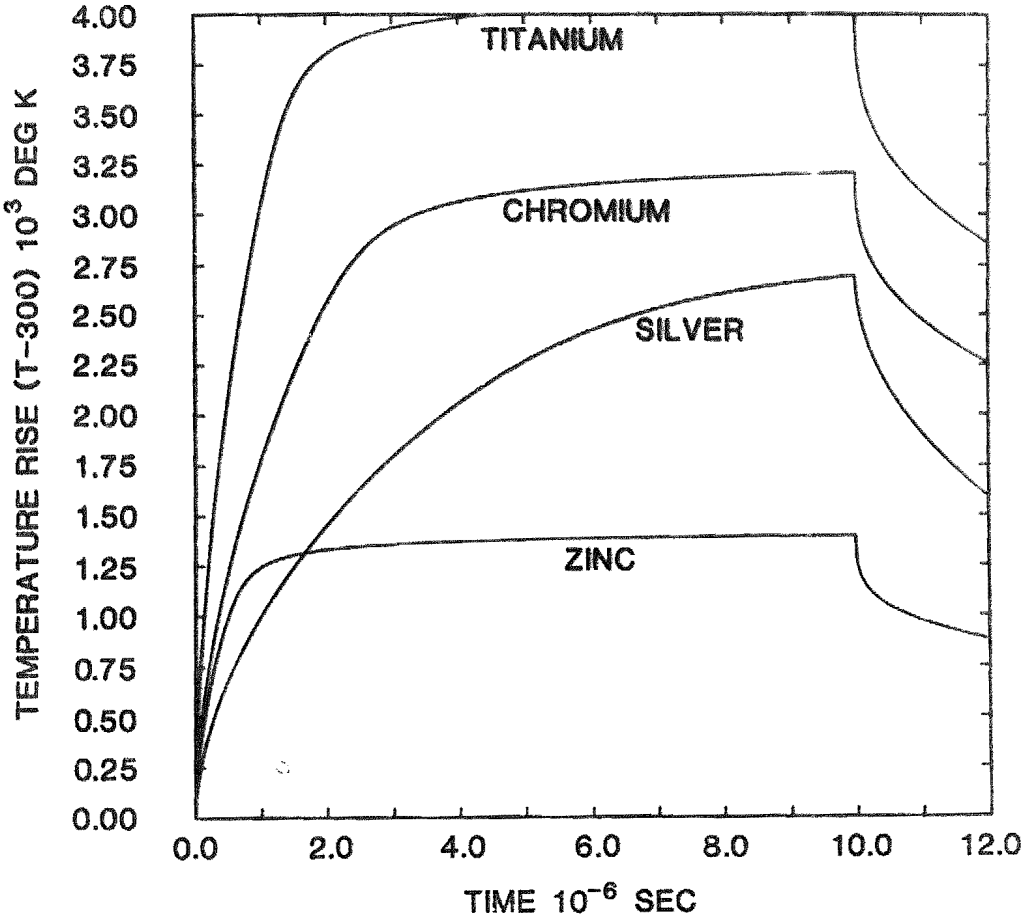

Figure 14. Additional examples of heating profiles for anode spots found on the indicated materials. These materials assume the same power input of 2 MW/cm^2 to the surface as in Fig. 13, but show more rapidly rising thermal profiles due to the material properties. Vaporization is effective later in the pulse to limit further temperature increases.

made at constant arc input power with no power feedback due to a limiting vapor flux. The thermal parameters used for the calculations are given in Table I. A specific power input to the anode spot in these calculations of 2×10^6 W/cm^2 and a power pulse of 10 microseconds duration have been assumed for the profiles in Fig. 13 and 14.

Summary and Discussion

A model has been presented for the thermal behavior of materials undergoing intense surface heating. The heat balance between the surface input power and thermal vaporization/dissociation and in some cases radiation losses has been described and applied to short pulsed vacuum arc anode phenomena. While the power input to the anode surface from the plasma in such an application has been parameterized, the model provides some insight into the plasma heat source term through observation of the anode spot temperatures. Specifically, the existence of a feedback mechanism to the arc power at high vapor flux levels is needed to describe the temperature risetime and vapor flux levels observed in experiments. Thus, the detailed thermal studies can complement plasma studies of anode-cathode behavior. The model described in this report extends previous thermal modeling to include effects of two constituent electrode materials. To do this, the effects of mass diffusion and concentration variations of the surface material have been included. The effect of vapor recondensation at the heated surface has also been considered. When compared to anode temperature and gas evolution measurements, the model appears to give a consistent description of the temperature pulse risetime, peak surface temperature and vapor flux.

Only a start has been made in comparing calculations with arc experiments because of the limited availability of experiments with temperature

diagnostics. Apparent difficulties remain in describing the temperature decay profiles at the end of the power pulse. Additional comparisons of thermal calculations to the arc measurements may be useful in resolving these differences.

The calculations show considerable sensitivity in thermal behavior to variations in the surface concentration and to the vapor sticking probability. Comparing such calculations to arc anode spot temperature and vapor flux measurements could contribute to understanding ion source behavior during both normal and abnormal conditions. In other areas, the modeling techniques developed here should be useful in studies of material performance under transient optical or electron heating.

Acknowledgment

The author wishes to express his thanks to J. C. Newton for numerous discussions of arc technology during this work and to M. Robertsen for the use of unpublished IR radiance data from arc heating tests. Suggestions for portions of this work and helpful comments on the manuscript were also contributed by G. W. McClure.

REFERENCES

1. J. T. Grissom and J. C. Newton, J. Appl. Phys. 45, 2885 (1974).

2. J. D. Cobine and E. E. Burger, J. Appl. Phys. 26, 895 (1955).

3. J. M. Lafferty Vacuum Arcs, Theory and Application, edited by J. M. Lafferty, J. Wiley and Sons New York (1980).

4. H. S. Carslaw and J. C. Jaeger, Conduction of Heat in Solids, Clarendon Press, Oxford, (1978).

5. R. B. Bird, W. E. Stewart and E. N. Lightfoot, Transport Phenomena John Wiley (1960).

6. J. L. Margrave, The Characterization of High Temperature Vapors, John Wiley New York (1967)

7. M. L. Lieberman and P. G. Wahlbeck, J. Phys. Chem. 69, 3514 (1965).

8. R. N. R. Mulford, USAEC Rept AECU-3813 A Review of the Rare Earth Hydrides, Off of Technical Information, Wash. DC (1958).

9. The Specific Heat of Metallic Elements and Alloys, Vol. 4, TPRC Data Series, IFI/Plenum, New York (1970).

10. Thermal Diffusivity, Vol. 10, TPRC Data Series, IFI/Plenum, New York, (1973).

11. L. P. Harris, Arc Cathode Phenomena, Ch. 4, Vacuum Arcs, Theory and Applications, ed. by J. M. Lafferty, J. Wiley and Sons, New York (1980).

12. G. W. McClure, J. Appl. Phys. 45, 2078 (1974)

13. H. C. Miller, IEEE Transaction on Plasma Science, Vol. PS5, 3 181 (1977).

14. M. M. Robertson Personal Communication.

15. J. C. Newton, Personal Communication. See also "Anode Surface Radiance from Microsecond Vacuum Arcs," SC-DR-72-0227, (July 1972).

16. H. T. Weaver, Phys. Rev. B 6, 2544 (1972).

17. A. N. Nesmeyanov, Vapor Pressure of the Chemical Element, Elsevier Pub. Co., New York (1963) p. 41.

18. M. E. Malinowski, "An Isotope Effect in the Pumping of Hydrogen by Titanium Thin Films," SAND77-8669 (August 1977).

19. M. Moss, "Heat Capacity and Thermal Diffusivity for ScD_x and ErD_x," SAND79-0249 (April 1979).

APPENDIX A

Listing of the program for surface temperature and vapor flux calculations.

```
00100 PROGRAM ARCT(INPUT,OUTPUT,TAPE40,ARCDAT,TAPE6=ARCDAT,TAPE16,TAPE17)
00110 DIMENSION FI(50 ),FO(501),T(501),STEMP(100),STIM(100),VFLUX(501)
00120 DIMENSION TIM(501),TITLE(5),XLAB(5),YLAB(5),YL(5),TL(5),PDW(4,501),PLAB(5)
00130 LOGICAL FIRST,PSWCH,FSWCH
00140 REAL M,MM
00150 DATA TITLE/50H
00160 DATA XLAB/50H                    TIME ()SEC
00170 DATA YLAB /50H          TEMPERATURE RISE (T-300)   ()DEG K
00180 DATA YL/50H               POWER ()J/CM2*SEC
00190 DATA TL/50H
00200 CALL HDCOPY(40)
00210C
00220C  ALL INPUTS CGS BUT ENERGY IN JOULES,CKIN-THERM COND J/(S*CM*C)
00230C  RHO-G/CM3, CP-HEAT CAP IN J/(G*C), M-MOLEC WT G/MOLE
00240C  RAD-SPOT RADIUS CM,  P-PRESSURE DYNES/CM2,FLUX IN MOLES/S*CM2
00250C
00260C FSWCH TRUE=MASS DIFF CALCULATED/FALSE=NO CONCENTRATION REDUCTION.
00270C PSWCH = TRUE FOR POWER CALCULATION: = FALSE FOR CONST POWER
00280C MOLES/CM**3 CONCENTRATION IN CINIT
00290C
00300C MULTIPLY A&B BY 2.303 & ADD 7.1953 TO B TO GET P IN DYNES/CM2
00310C WITH NATURAL LOGS FROM P IN MM HG AND LOG BASE 10 PARAMETERS.
00320 201 READ(6,*)ICRD
00330 IF(EOF(6).EQ.1) GO TO 254
00340 200 FORMAT(1X,6A10)
00350 BACKSPACE 6
00360 IF(ICRD.EQ.1)READ(6,*)ICRD,ICASE,TMAX,PMAX,TIMMAX
00370 IF(ICRD.EQ.1)FIRST=.T.
00380 IF(ICRD.EQ.1) ITIMES=0
00390 IF(ICRD.EQ.2)READ(6,200)(TITLE(I),I=1,4)
00400 IF(ICRD.EQ.3)READ(6,200)(TL(I),I=1,4)
00410 IF(ICRD.EQ.4)READ(6,*)ICRD,FSWCH,PSWCH,DTIM,PL,PIN,RAD,FLUX0
00420 IF(ICRD.EQ.5)READ(6,*)ICRD,RHO,CP,CKIN,A,B,M,ALPHA
00430 IF(ICRD.EQ.6)READ(6,*)ICRD,CONL,CONH,CON0,AM,BM,MM,HDIFF
00440 IF(ICRD.EQ.9)READ(6,200)TRASH
00450 IF(ICRD.NE.9)GO TO 201
00460 IF(MM.EQ.0) MM=1
00470 IF(M.EQ.0) M=1
00480 CONC=CON0
00490 FLUX=0
00500 CK=CKIN
00510 D=CK/(RHO*CP)
00520 IMAX=500
00530 I=0
00540 ITIMES=ITIMES+1
00550 IF(ITIMES.GT.4)GOTO 202
00560 R=8.36
00570 COEF=SQRT(3.1416*CK*RHO*CP)
00580 COEF=1./COEF
00590 FO(1)=0
00600 TIM(1)=0
00610 VFLUX(1)=0
00620C
00630C TIME ITERATION LOOP
00640 1 I=I+1
00650 IF(I.GT.IMAX) GO TO 3
00660 TIM(I+1)=DTIM*I
00670 FI(I)=0
00680 IF(PSWCH)19,18
00690C
00700C COMPUTE CONSTANT INPUT POWER.
00710 18 IF(TIM(I).LE.PL) FI(I)=PIN
00720 GO TO 22
00730C
```

```
00740C CALCULATE POWER FOR CONST. FLUX.
00750 19 IF((FLUX/FLUX0).LE..50) 20,21
00760 20 IF(TIM(I).GE.PL) GO TO 22
00770 FI(I)=PIN
00780 GO TO 22
00790 21 DFDT=-FLUX/(2.*T(I-1))-FLUX*A/(T(I-1)**2)
00800 FLCOR=(FLUX0-FLUX)/DFDT
00810 DF=(T(I-1)-T(I-2)-FLCOR)/(COEF*SQRT(DTIM))
00820 FI(I)=FI(I-1)-DF
00830 IF(FI(I).LT.0) FI(I)=0
00840 IF(FI(I).GT.PIN) FI(I)=PIN
00850 22 CONTINUE
00860 IF(TIM(I).GE.PL) FI(I)=0
00870 POW(ITIMES,I)=FI(I)
00880C
00890C CALCULATE SURFACE TEMPERATURE
00900 T(I)=0
00910 DO 2 II=1,I
00920 S1=1.-EXP(-(RAD**2)/(4.*D*TIM(II+1)))
00930 IIT=I-II+1
00940 F=FI(IIT)-FO(IIT)
00950 T(I)=T(I)+S1*COEF*F*DTIM/SQRT(TIM(II+1))
00960 2 CONTINUE
00970C
00980C CODE TO COMPUTE POWER LOSS FROM SURFACE BY EVAPORATION
00990C COMPUTE VAPOR FLUX
01000C FIRST COMPUTE CONCENTRATION OF  EVAP SPECIES AT SURFACE.
01010 IF(.N.FSWCH)GO TO 71
01020 FLUXINT=0
01030 DO 70 II=1,I
01040 IIT=I-II+1
01050 FLUXINT=FLUXINT+VFLUX(IIT)*DTIM/SQRT(TIM(II+1))
01060 70 CONTINUE
01070 CONC=CON0-FLUXINT/SQRT(3.14159*HDIFF)
01080 IF(CONC.LE.0) CONC=0
01090 71 P=EXP(A/(T(I)+300.)+B)
01100 IF(.N.FSWCH) GO TO 72
01110 IF(CONC.LT.CONL) P=P*(CONC/CONL)**2
01120 IF(CONC.GT.CONH) P=P*(CONC/CONH)**2
01130C  HVAP IN J/MOLE
01140 72 HVAP=-A*R
01150 FLUX=SQRT(8./(3.1416*R*(T(I)+300.)*M*1.E07))
01160 FLUX=FLUX*ALPHA*P/4.
01170 PM=EXP(AM/(T(I)+300)+BM)
01180 IF(PM.EQ.1) PM=0
01190 HVAPM=-AM*R
01200 FLUXM=SQRT(8/(3.1416*R*(T(I)+300)*MM*1.E07))
01210 FLUXM=FLUXM*ALPHA*PM/4
01220 VFLUX(I+1)=FLUX+FLUXM
01230C  FLUX IN MOLES/(CM2*S)
01240C  OUTPUT POWER IN WATTS/CM2
01250 EVAP=FLUX*(HVAP+1.5*R*T(I))+FLUXM*(HVAPM+1.5*R*T(I))
01260C
01270C COMPUTE RADIATION LOSS TERM
01280 FRAD=5.6697E-12*(T(I)+300.)**4
01290 FO(I+1)=EVAP+FRAD
01300C
01310C PRINT OUTPUT
01320 IF(I.EQ.1)10,11
01330 10 PRINT*," "
01340 PRINT*," "
01350 PRINT*, " CK= " ,CK, " RHO= " ,RHO, " CP= " ,CP, " D= " ,D
01360 PRINT*, "LN P =A/T +B  BASE E WITH A=" ,A, " B=" ,B," M=",M
01370 PRINT*, "        FOR SECOND COMPONENT  A= ",AM, " B= ",BM," M= ",MM
01380 PRINT*, " PIN= " ,PIN, " PL= " ,PL,"  HVAP=",HVAP,"  HVAP2=",HVAPM
01390 PRINT*," CON0= ",CON0," CONL= ",CONL," CONH= ",CONH," HDIFF= ",HDIFF
```

```
01400 PRINT*," ALPHA= ",ALPHA
01410 PRINT*," "
01420 PRINT*,"SURFACE  TIME       ENERGY FLUX AT SURFACE       VAPOR    VAPOR  CONC
01430+   FL"
01440 PRINT*," TEMP    SEC    TOT OUTPUT  INPUT    RADIANT    FLUX     PRESS  MOLE
01450+S  UX"
01460 PRINT*,"  C                 W/CM2      W/CM2     W/CM2  MOL/CM2-S BYN/CM2  /CM
01470+3  2 "
01480 PRINT*," "
01490 11 J=(I-1)/50+1
01500 BJ=J
01510 AJ=I-1
01520 AJ=AJ/50+1
01530 IF(AJ.EQ.BJ)12,13
01540 12 CONTINUE
01550 IF(FLUXM.LT.1.E-7) FLUXM=0
01560 PRINT99,T(I),TIM(I),FD(I),FI(I),FRAD,FLUX,P  ,CONC,FLUXM
01570 99 FORMAT(F5.0,1X,E9.3,3(1X,E9.3),2(1X,E8.2),F5.3,1X,E7.2)
01580 100 FORMAT(7(1X,E10.4))
01590 7 STEMP(J)=T(I)
01600 STIM(J)=TIM(I)
01610 13 CONTINUE
01620 GO TO 1
01630 3 CONTINUE
01640 IF(FIRST) 5,6
01650 5 FIRST=.F.
01660 CALL PLOTPQ(0,0,TIM,T,IMAX,1,1,1,1H ,TITLE,XLAB,YLAB,1,1,0.,TIMMAX
01670+,1,0.,TMAX)
01680 GO TO 4
01690 6 CALL PLOTPQ(0,0,TIM,T,IMAX,1,1,1,1H ,TITLE,XLAB,YLAB,0,1,0.
01700+,TIMMAX,1,0.,TMAX)
01710 4 CONTINUE
01720 IF(ITIMES.EQ.1) PRINT200,(TITLE(I),I=1,5)
01730 IF(ITIMES.EQ.ICASE) GO TO 202
01740 GO TO 201
01750 202 PRINT*,"IS TEMPERATURE OVERLAY FROM TAPE16 WANTED?"
01760 READ 250,ANS
01770 250 FORMAT(1A1)
01780 IF(ANS.NE.1HY)GO TO 251
01790 I=0
01800 REWIND 16
01810 READ(16,200),(RLAB(I),I=1,5)
01820 PRINT 200,(RLAB(I),I=1,5)
01830 253 I=I+1
01840 READ(16,*) FI(I),T(I)
01850 IF(EOF(16).EQ.1)252,253
01860 252 CALL PLOTPQ(0,0,FI,T,I,1,0,0,1H*,TITLE,XLAB,YLAB,0,1,0.,TIMMAX
01870+,1,0.,TMAX)
01880 251 CONTINUE
01890 DO 73 IPL=1,ITIMES
01900 DO 75 I=1,IMAX
01910 FI(I)=POW(IPL,I)
01920 75 CONTINUE
01930 IF(IPL.NE.1) GO TO 74
01940 CALL PLOTPQ(0,0,TIM,FI,IMAX,1,1,1,1H ,TL,XLAB,YL,1,1,0.,TIMMAX
01950+,1,0.,PMAX)
01960 GO TO 73
01970 74 CALL PLOTPQ(0,0,TIM,FI,IMAX,1,1,1,1H ,TL,XLAB,YL,0,1,0.
01980+,TIMMAX,1,0.,PMAX)
01990 73 CONTINUE
02000 PRINT 200,(TL(I),I=1,5)
02010 GO TO 201
02020 254 CALL EXTFLM(0)
02030 END
```

UNLIMITED RELEASE

Distribution:

Las Alamos National Scientific Laboratory
P. O. Box 1662
Los Alamos, NM 87544
Attn: T. E. Larson (MS 920)

Lawrence Livermore National Laboratory
P. O. Box 808
Livermore, CA 94550
Attn: C. A. Colmenares (L-325)

General Electic Leutron Devices Department
St. Petersburg, FL 33733
Attn: D. H. Ahmann
W. C. Brown
B. E. Day
W. E. Ierna
H. C. Miller
J. L. Provo
A. S. Medvedeff
W. D. Wannamaker
E. Noey

8340 W. Bauer
8341 W. D. Wilson
Attn: M. I. Baskes
M. E. Stoll
G. J. Thomas
8342 C. Hartwig
8347 K. Wilson
Attn: M. E. Malinowski
2300 J. C. King
2350 J. T. Grissom
2351 R. A. Damerow
2352 F. M. Bacon
2352 D. F. Cowgill
2352 J. C. Newton
2353 J. T. Cutchen
2353 J. T. Cutchen (5 for further distribution to UK)
2354 B. E. Barnaby
2355 H. M. Bivens
2516 W. G. Perkins
4240 G. W. Kuswa
4244 G. W. McClure
5130 G. A. Samara
5131 B. Morosin
5132 P. M. Richards
5500 O. E. Jones
5510 D. B. Hayes
5520 T. B. Lane
5530 W. Herrmann
5531 S. W. Key
5533 A. J. Chabai
5534 J. R. Asay
5534 D. A. Benson (10)
5824 J. N. Sweet
5824 J. A. Koski
8214 P. A. Childers
3141 L. J. Erickson (3)
3151 W. L. Garner (5)
For DOE/TIC
3154-3 R. P. Campbell (25)
For DOE/TIC